Dalton Transactions

ROYAL SOCIETY OF CHEMISTRY

PAPER

View Article Online
View Journal

Cite this: DOI: 10.1039/d1dt00806d

Al_2O_3/CuI/PANI nanocomposite catalyzed green synthesis of biologically active 2-substituted benzimidazole derivatives†

Sahil Kohli,[a,b] Garima Rathee,[a] Sunita Hooda*[b] and Ramesh Chandra*[a]

Received 10th March 2021,
Accepted 23rd April 2021

DOI: 10.1039/d1dt00806d

rsc.li/dalton

This work is generally focused on the synthesis of an efficient, reusable and novel heterogeneous Al_2O_3/CuI/PANI nanocatalyst, which has been well synthesized by a simple self-assembly approach where aniline is oxidized into PANI and aniline in the presence of KI also acts as a reductant. The nanocatalyst was well characterized by XRD, FTIR, SEM, EDX, TEM, BET and XPS techniques. In this study, the fabricated material was employed for the catalytic one-pot synthesis of 2-substituted benzimidazoles *via* condensation between *o*-phenylenediamine and aldehydes in ethanol as a green solvent. The present method is facile and offers several advantages such as high % yield, less reaction time, and no use of additive/bases. Also, the catalyst showed better values of green metrics including low E-factor: 0.17, high reaction mass efficiency: 85.34%, high carbon efficiency: 94%, and high process mass intensity: 1.17.

Introduction

N-Heterocycles have always been an interesting class of organic compounds. Among various N-heterocycles, the benzimidazole scaffold has efficiently attracted the interest of researchers across the globe owing to its numerous biological characteristics such as antiviral,[1] anticancer,[2] anti-inflammatory,[3] antihypertensive,[4] antifungal[5] and antiulcer activities.[6] Some of the biologically active benzimidazole molecules are shown in Fig. 1. The derivatives of benzimidazole are also recognized as intermediates in synthetic chemistry and as ligands in asymmetric catalysis.[7] Moreover, they are also advantageous in the fields of dyeing, chemosensing, fluorescence and corrosion science.[8] The classical way for the fabrication of benzimidazole derivatives includes the reaction of *o*-phenylenediamine with carboxylic acids or their derivatives at high temperature under conditions of strong acidic media.[9] However, such traditional methods suffer from various disadvantages such as, usage of inorganic acids, waste production in higher amounts, difficulty in the catalyst's reusability and low atom economy.[10]

In the past few years, nanomaterials have emerged as better alternatives for several organic transformations as compared to conventional materials. Such advanced applicability of nanomaterials in the field of heterogeneous catalysis and as catalyst supports is due to their higher surface area, and unique textural and structural properties.[11] Moreover, supported metal nanoparticles have attracted more significant attention rather than unsupported metal nanoparticles for catalytic applications because of their large surface and volume ratio. Furthermore, the intramolecular bonding between metal–metal, surface interaction and interaction between metal–support make the supported metal nanoparticles effective.[12] Alumina is the most commonly used ceramic material of oxide which acts as a cata-

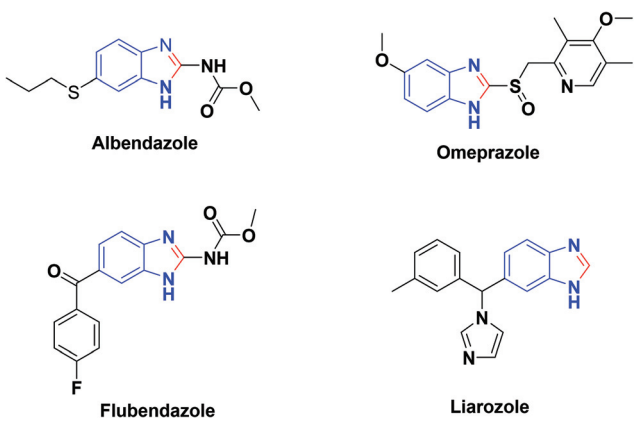

Fig. 1 Biologically active molecules containing benzimidazole heterocyclic scaffolds.

[a]Drug Discovery & Development Laboratory, Department of Chemistry, University of Delhi, Delhi-110007, India. E-mail: acbrdu@hotmail.com, rameshchandragroup@gmail.com

[b]Department of Chemistry, Acharya Narendra Dev College, University of Delhi, Delhi-110019, India. E-mail: hooda_sunita@hotmail.com

†Electronic supplementary information (ESI) available: SEM and XRD of the recycled catalyst; green chemistry metric calculations, spectral data of compounds, and ^{1}H NMR and ^{13}C NMR spectra of all compounds. See DOI: 10.1039/d1dt00806d

lyst support because of its high thermal and chemical stability, well-defined porous structure and high specific surface areas.[13] Alumina provides sites for anchoring various metallic species in various applications such as Fischer–Tropsch synthesis using the CoPt/Al_2O_3 nanocatalyst,[14] oxidation of benzene by Pt/Al_2O_3 catalysts,[15] dry reforming of methane over the Ni–Cu/Al_2O_3 catalyst,[16] *etc*. Furthermore, polyaniline is an essential conducting polymer because of its non-toxic behaviour, high stability, low cost and facile synthesis, and redox properties.[17] It is useful as a support for various metal catalysed organic reactions in modern organic synthesis.[18]

Copper nanoparticles are mainly attractive because of their high abundance in nature, inexpensive cost and several methods of preparation.[19–22] Copper is a 3d transition metal which exhibits variable oxidation states from 0 to +3 and because of this property, copper based materials can undergo various organic transformations through one- and two-electron pathways.[23] Copper based nanomaterials have a wide range of applications in organic reactions including various cross coupling,[24,25] oxidative coupling,[26] and multicomponent reactions.[27]

Our research group has previously successfully reported the fabrication of multiple heterogeneous nanocatalysts for the one-pot synthesis of various biologically significant organic scaffolds such as xanthenes, 1,4-dihydropyridines, polyhydroquinolines, and 4H-pyrans.[28,29] Herein we introduce a novel Al_2O_3/CuI/PANI catalyst for the synthesis of 2-substituted benzimidazoles from *o*-phenylenediamine and aldehydes as starting materials at room temperature under greener conditions. During the process of fabrication, the Cu^{2+} ions get anchored on the surface of Al_2O_3 forming an Al_2O_3–Cu^{2+} complex. Furthermore, aniline is oxidized into PANI and Cu^{2+} is reduced to Cu^{+} in the presence of aniline as a reductant. The obtained catalyst was characterized by techniques such as XRD, FTIR, SEM, EDX, TEM, XPS and BET. The obtained material was found to be steady under the employed reaction conditions and was easily recovered and recycled up to five times without any considerable loss in the yield.

Results and discussion

Development and characterization of the Al_2O_3/CuI/PANI nanocomposites

Initially, 100 mg of Al_2O_3 was added into 40 mL of water. Then 3.04 g of $CuSO_4{\cdot}5H_2O$ was added to this solution and heated over a water bath at 60 °C overnight for the accumulation of Cu^{2+} ions on the surface of Al_2O_3 under continuous stirring. Cu^{2+}–Al_2O_3 was collected and washed 3–4 times with distilled water. The obtained Cu^{2+}–Al_2O_3 compound was again added into 40 mL of 0.5 M aq. solution of KI and 0.4 mL of aniline was added into this solution under constant stirring and the obtained solution was further stirred at room temperature for 24 hours. Lastly, the purple-black precipitate was removed by centrifugation and washing was done with distilled water followed by ethanol. The nanocatalyst was dried at 60 °C overnight (Fig. 2).

The synthesized Al_2O_3/CuI/PANI nanocatalyst was characterized by XRD, FTIR, SEM, EDAX, TEM, BET and XPS techniques.

The powder XRD pattern of the Al_2O_3/CuI/PANI nanocatalyst is shown in Fig. 3. The peaks at 2θ = 25.5, 29.6, 42.2, 50.0, 61.2, 67.4 and 77.3 correspond to copper iodide which could be confirmed by comparing it with the JCPDF file (06-0246). The PANI peak does not appear in the pattern at 2θ = 25 because the peak is covered by the high intensity of the CuI peak [111] at 25.5.[30]

Fig. 4shows the FTIR spectrum of Al_2O_3/CuI/PANI which exhibits peaks at 1591 and 1475 cm^{-1} related to the C=C stretching vibrations of quinoid and benzenoid units. The peaks at 1331 cm^{-1} and 1296 cm^{-1} are due to the deformations of the C–N bond and the stretching vibrations of the

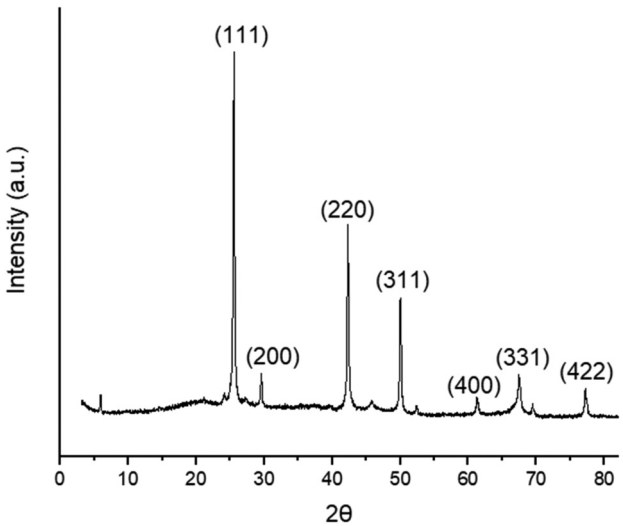

Fig. 3 XRD spectra of the nanocatalyst.

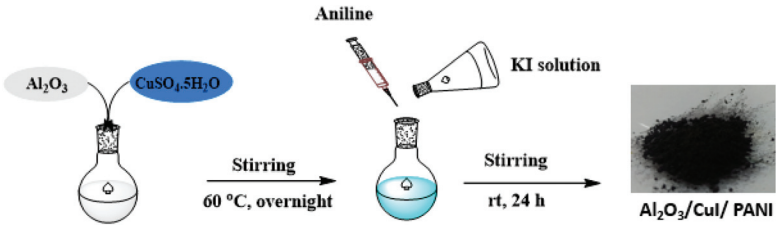

Fig. 2 Schematic diagram for the synthetic development of the Al_2O_3/CuI/PANI nanocatalyst.

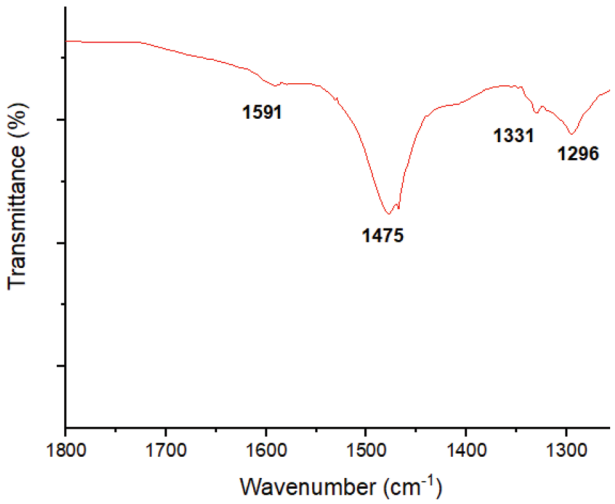

Fig. 4 FTIR spectra of the nanocatalyst.

C–N bond respectively.[30] These values in the spectrum confirm the presence of PANI.

The SEM pattern was analysed for studying the morphology of the Al_2O_3/CuI/PANI nanocomposite. The SEM images are displayed in Fig. 5 and Fig. 6 illustrates the TEM images of the Al_2O_3/CuI/PANI nanocatalyst at 200 nm and 100 nm. For the size determination of the nanoparticles, the size of the discrete particles was measured using TEM images and the size was found to be in the range of 25–40 nm. Also, these images clearly indicate that CuI has been accumulated on the surface of alumina.

The EDX spectra of Al_2O_3@CuI@PANI are presented in Fig. 7 which shows the presence of copper, iodide, aluminium, oxygen, nitrogen and carbon at 15.41, 23.51, 19.52, 3.48, 13.26 and 24.83 wt% respectively.

The surface composition of the synthesized Al_2O_3/CuI/PANI samples was examined by XPS as shown in Fig. 8g. This composite is mainly composed of Cu, I, Al, O, N and C. In the high resolution spectrum the Cu $2p_{1/2}$ and Cu $2p_{3/2}$ lines appear at 952.3 and 932.4 eV respectively which confirms that copper exists in the +1 oxidation state (Fig. 8a).[31] The XPS of I $3d_{3/2}$ and I $3d_{5/2}$ lines at 631.0 and 619.5 eV matches with the reported data for CuI nanoparticles (Fig. 8b). The binding energy value of the Al 2p and O 1s peaks at 74.4 and 531.0 eV corresponds to the presence of Al_2O_3 and oxide respectively as shown in Fig. 8c and d. The carbon (N 1s) and nitrogen (C 1s) atoms of PANI are located at 399.6 and 284.8 eV as shown in Fig. 8e and 8f.[30]

The N_2 adsorption–desorption isotherm and pore radius of the Al_2O_3/CuI/PANI nanocatalyst are shown in Fig. 9. It is attributed to the H2 (b) hysteresis loop of the isotherm. The nanocatalyst Al_2O_3/CuI/PANI has a BET surface area: 59.02 m^2 g^{-1}, pore radius: 7.34 nm, and pore volume: 0.22 cm^3 g^{-1}.

Al_2O_3/CuI/PANI as the nanocatalyst for the synthesis of benzimidazole derivatives

Initially, the reaction of *o*-phenylenediamine (**1**) and 4-methylbenzaldeyde (**2**) using the Al_2O_3/CuI/PANI catalyst (5 mg)

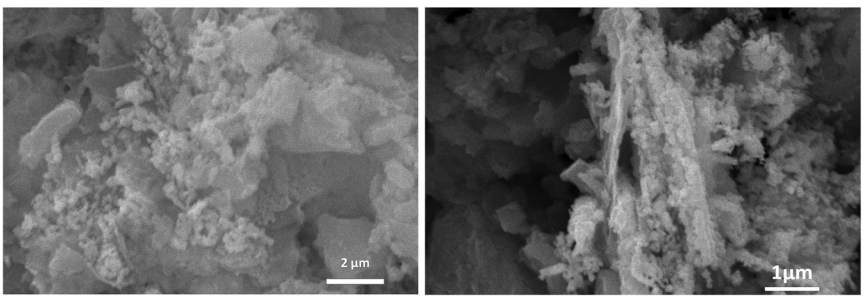

Fig. 5 SEM images of the Al_2O_3/CuI/PANI nanocatalyst.

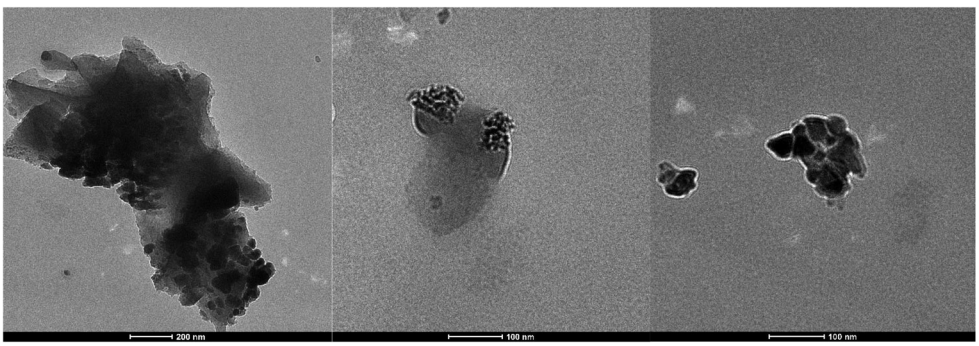

Fig. 6 TEM images of the Al_2O_3/CuI/PANI nanocatalyst.

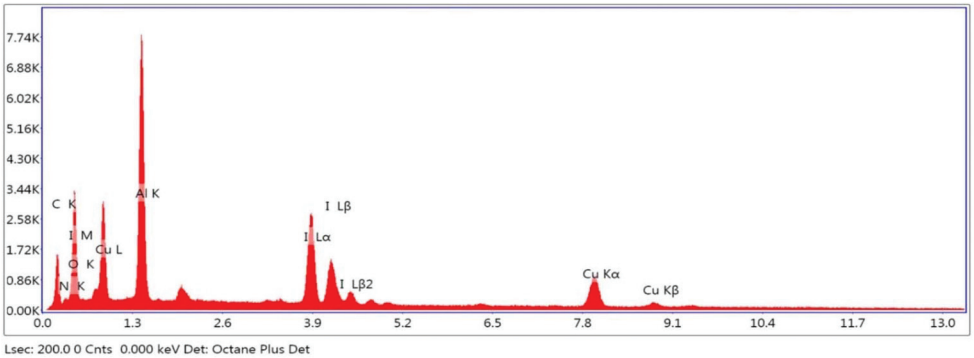

Fig. 7 EDX of the Al_2O_3/CuI/PANI nanocatalyst.

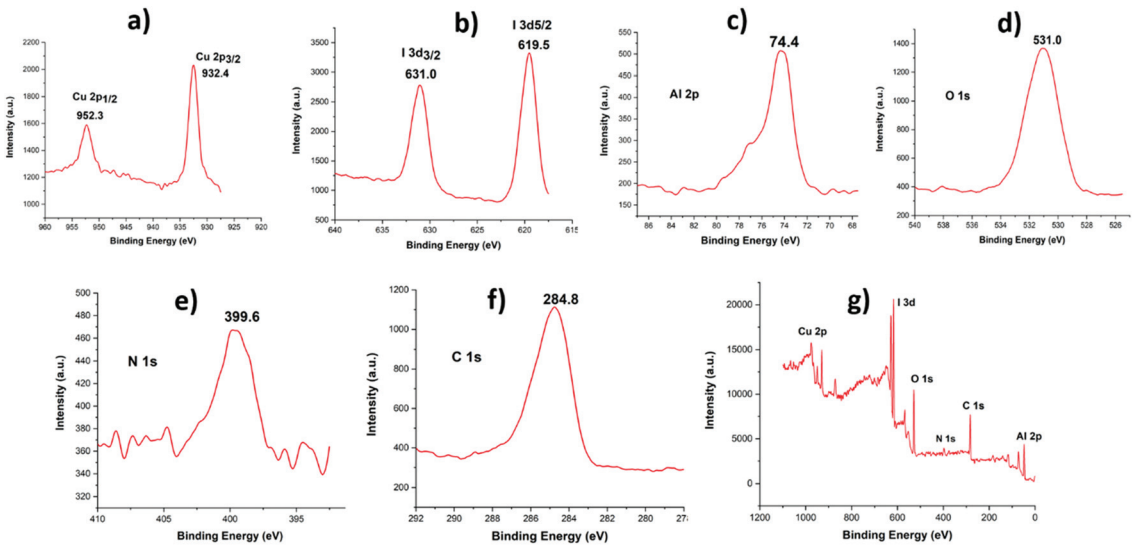

Fig. 8 High resolution XPS of (a) Cu; (b) I; (c) Al; (d) O; (e) N; (f) C; (g) Al_2O_3/CuI/PANI nanocomposite.

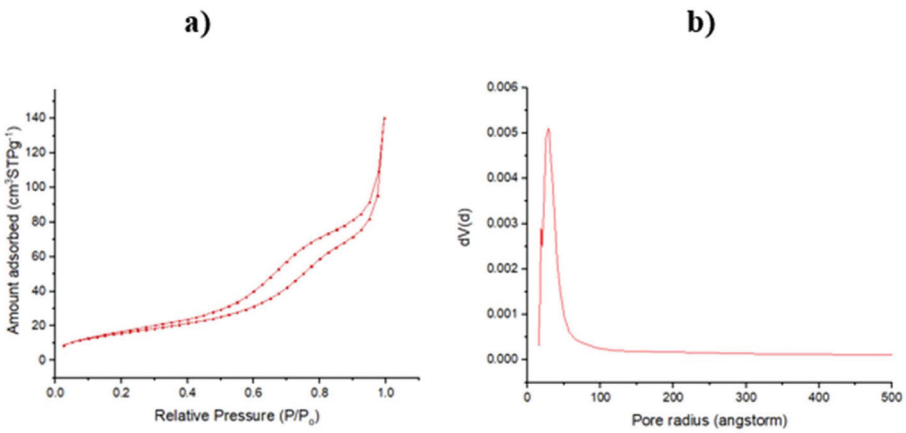

Fig. 9 (a) Representative isotherm of N_2 adsorption–desorption; (b) Al_2O_3/CuI/PANI nanocatalyst pore radius.

under neat conditions and in different solvents at room temperature was carried out (Table 1). There was no formation of the product in toluene (entry 1, Table 1). The reaction was performed in polar aprotic solvents such as THF, DMF, acetonitrile and DMSO. In THF and acetonitrile, the product was formed in a trace quantity while in DMF and DMSO the pre-

Table 1 Optimization of the Al_2O_3/CuI/PANI nanocatalyst for the synthesis of benzimidazole derivatives using *o*-phenylenediamine (**1**) and 4-methylbenzaldehyde (**2c**)[a]

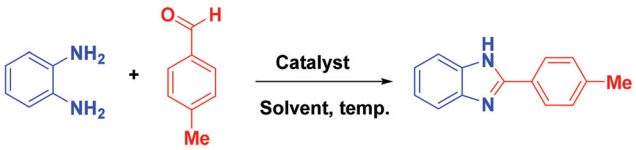

1 **2c** **3c**

Entry	Catalyst (mg)	Solvent	Temp (°C)	Time (h)	Yield (%)
1	Al_2O_3/CuI/PANI (5)	Toluene	rt	24	—
2	Al_2O_3/CuI/PANI (5)	THF	rt	8	Trace amount
3	Al_2O_3/CuI/PANI (5)	Acetonitrile	rt	8	Trace amount
4	Al_2O_3/CuI/PANI (5)	DMF	rt	8	47
5	Al_2O_3/CuI/PANI (5)	DMSO	rt	8	61
6	Al_2O_3/CuI/PANI (5)	Neat	rt	24	68
7	Al_2O_3/CuI/PANI (5)	Water	rt	24	—
8	Al_2O_3/CuI/PANI (5)	EG	rt	8	77
9	Al_2O_3/CuI/PANI (5)	Methanol	rt	1	71
10	**Al_2O_3/CuI/PANI (5)**	**Ethanol**	**rt**	**1**	**92**
11	Al_2O_3/CuI/PANI (5)	Ethanol	50	1	92
12	Al_2O_3/CuI/PANI (5)	Ethanol	60	1	92
13	Al_2O_3/CuI/PANI (10)	Ethanol	rt	1	92
14	Al_2O_3/CuI/PANI (20)	Ethanol	rt	1	92
15	CuI salt (5)	Ethanol	rt	1	35
16[b]	Al_2O_3/CuI/PANI (5)	Ethanol	rt	1	—

[a] Reaction conditions: *o*-phenylenediamine **1** (0.5 mmol), aldehyde **2** (0.5 mmol), Al_2O_3/CuI/PANI (5–20 mg) and solvent (3 ml) were stirred at suitable temperature. [b] Reaction under a N_2 atmosphere.

ferred product was 47% and 61% respectively (entries 2–5, Table 1).

When neat conditions and green solvents such as water, ethylene glycol (EG), and ethanol were used to find sustainable and green conditions of the reaction, it was observed that no reaction takes place in water (entry 7, Table 1) while upon using EG, methanol and ethanol, the formed product was 77%, 71% and 92% respectively (entry 8–10, Table 1). Under neat conditions, the formed product was 68% (entry 6, Table 1). So the best suitable solvent to afford the product was found to be ethanol (entry 10, Table 1). Following this, the influence of temperature was studied; an increase in the temperature results in the same yield in 1 h (entry 11 and 12, Table 1). Then upon increasing the amount of the catalyst, the yield was found to be the same (entry 13 and 14, Table 1). Then the yield was found to be 35% when the CuI salt was used (entry 15, Table 1). The reaction does not take place when performed in an inert atmosphere of N_2 (entry 16, Table 1). Therefore, the suitable conditions for the reaction were 5 mg of the Al_2O_3/CuI/PANI nanocatalyst in ethanol as a solvent at room temperature for 1 h.

2-Benzimidazole derivatives were synthesized under the suitable conditions for the reaction as shown in Table 2. Different benzaldehydes were used with an excellent yield of the preferred product in all products (**3a–3n**).

The plausible mechanism of the Al_2O_3/CuI/PANI nanocomposite catalyzed synthesis of 2-substituted benzimidazole is shown in Fig. 10. The first step is the activation of aldehyde by the catalyst followed by the formation of imine with one of the amino groups. The next step involves the attack of another amino group to the imine resulting in cyclization followed by aerial oxidation resulting in 2-substitued benzimidazole.[32]

Next we studied the recyclability of the catalyst. Once the reaction was completed, the catalyst was isolated from the reaction mixture by adding ethanol followed by centrifugation and then it was washed with ethanol many times and dried overnight in an oven. The material was used for five cycles more without any appreciable decrease in the yield which shows a greener path for the synthesis of benzimidazole derivatives as shown in Fig. 11. The SEM and XRD spectra were compared for the recycled catalyst and the fresh catalyst after five consecutive cycles which shows no loss in the catalytic activity (ESI S3 Fig. S1 and S2†).

The current methodology is sustainable and green as it can be seen from the values of green metrics (calculations in the ESI document S4 and S5†) which are near to ideal values (Table 3).

Experimental section

Procedure for 2-(*p*-methylphenyl)-benzimidazole synthesis (3a)

In a round bottom flask, *o*-phenylenediamine (0.5 mmol), 4-methyl benzimidazole (0.5 mmol) and Al_2O_3/CuI/PANI nano-

Table 2 Al_2O_3/CuI/PANI nanocatalyzed synthesis of 2-benzimidazole derivatives[a]

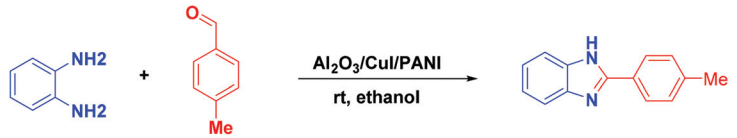

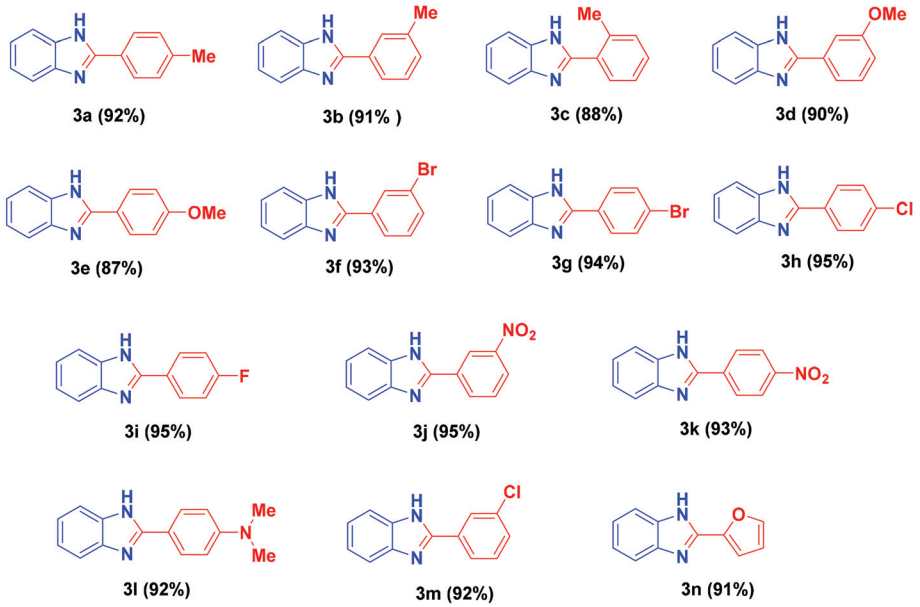

[a] Reaction conditions: *o*-phenylenediamine **1** (0.5 mmol), aldehyde **2** (0.5 mmol), Al_2O_3/CuI/PANI (5 mg) and ethanol (3 ml) were stirred at room temperature for 1 h.

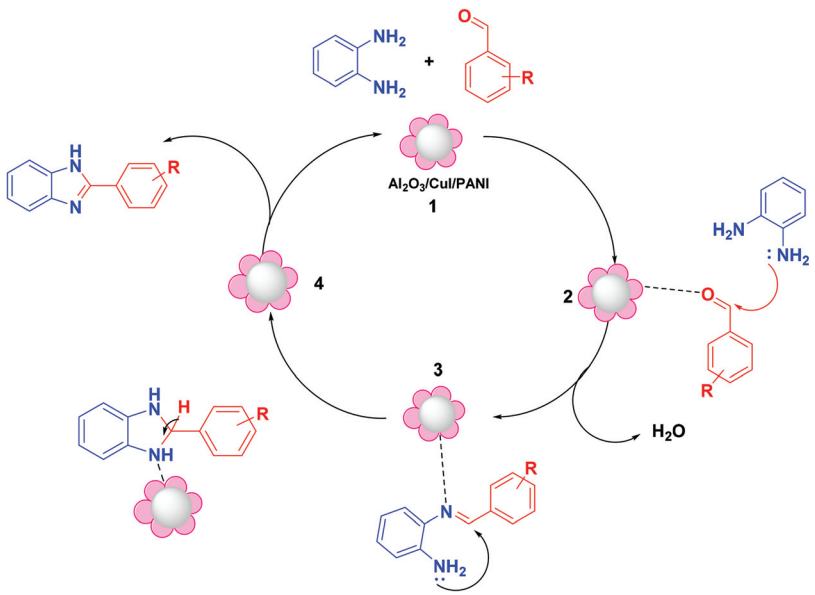

Fig. 10 Possible mechanism for the reaction catalysed by Al_2O_3/CuI/PANI.

particles (5 mg) were added in ethanol (3 mL) and stirred at room temperature for an hour. The reaction was monitored by TLC with ethyl acetate/hexane as the eluent. After the completion of the reaction, the catalyst was filtered and the residue was extracted with ethyl acetate followed by column chromatography to obtain a purified product (Table 4).

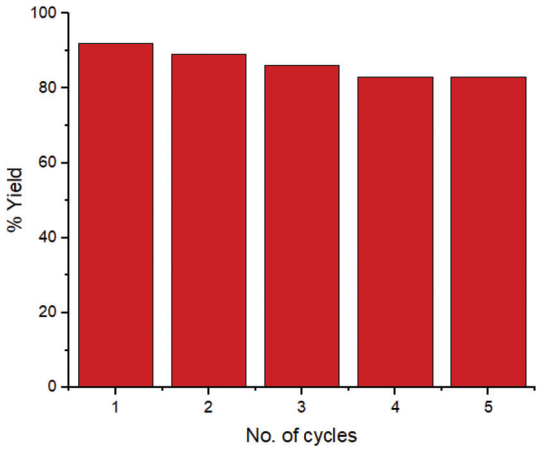

Fig. 11 Recyclability of the Al_2O_3/CuI/PANI nanocatalyst for compound **3a** synthesis.

Table 3 Values of green metrics

S. no	Catalyst	E factor	Process mass intensity	Reaction mass efficiency
1.	Al_2O_3/CuI/PANI	0.17	1.17	85.34%

Table 4 Comparative study of various catalysts for the synthesis of 2-(*p*-methylPhenyl)-benzimidazole

Entry	Catalyst	Solvent/ condition	Time	Yield (%)	Ref.
1	TBN	THF, rt, O_2	2 h	79	33
2	Pt/TiO_2	Mesitylene, rt	1 h	75	34
3	CuI NPs	CH_3CN, rt, O_2	1.5 h	89	35
4	$CuFe_2O_4$	Toluene, 110 °C, O_2	24 h	53	36
5	$ClSO_3H$	2-Propanol, rt	2 h	88	37
6	a-MoO_3 nanobelts	50° C, *t*-BuOOH	40 min	90	38
7	CuO np/silica	Methanol, rt	6 h	87	39
8	Al_2O_3/CuI/PANI	Ethanol, rt	1 h	92	This study

Conclusion

In summary, we designed a novel Al_2O_3/CuI/PANI nanocomposite which is found to be an efficient and versatile nanocatalyst for the synthesis of benzimidazole by reaction between *o*-phenylenediamine and aldehydes in ethanol as a green solvent. This method is advantageous due to its simple procedure for catalyst preparation, ambient reaction conditions and no use of additive/bases with ideal values of green metrics. The nanocatalyst was easily recovered and reused for five constant sets of cycles without much decrease in the catalytic activity.

Spectral data of the compounds

2-(*p*-Methylphenyl)-benzimidazole (3a)[40]

Colourless solid; yield: 92%; mp = 267–269 °C; ^{1}H NMR (DMSO-d_6, 400 MHz): δ 12.87 (s, 1H), 8.09–8.07 (d, J = 8.25 Hz, 2H), 7.58 (s, 2H), 7.37–7.35 (d, J = 8.00 Hz, 2H), 7.21–7.18 (m, 2H), 2.38 (s, 3H). ^{13}C NMR (DMSO-d_6, 100 MHz): δ 151.83, 140.02, 129.97, 127.89, 126.84, 122.39, 21.44; HRMS (ESI) calcd $[M + H]^+$ 209.1073; found 209.1077; Anal. Calcd for $C_{14}H_{12}N_2$: C, 80.74; H, 5.81; N, 13.45; found C, 80.72; H, 5.79; N, 13.46.

2-(*m*-Methylphenyl)-benzimidazole (3b)[45]

White solid; yield: 91%; mp = 213–215 °C; ^{1}H NMR ($CDCl_3$, 400 MHz): δ 7.88 (s, 1H), 7.83–7.82 (d, J = 7.56 Hz, 1H), 7.56–7.54 (m, 2H), 7.18–7.15 (m, 3H), 7.12–7.09 (d, J = 7.70 Hz, 1H), 2.15 (s, 3H). ^{13}C NMR ($CDCl_3$, 100 MHz): δ 152.26, 139.19, 138.73, 131.50, 129.22, 127.94, 124.19, 123.40, 115.34, 21.50. Anal. Calcd for $C_{14}H_{12}N_2$: C, 80.74; H, 5.81; N, 13.45; found C, 80.75; H, 5.80; N, 13.47.

2-(*o*-Methylphenyl)-benzimidazole (3c)[40]

Colourless solid; yield: 88%; mp = 223–225 °C; ^{1}H NMR ($CDCl_3$, 400 MHz): δ 7.58–7.55 (m, 4H), 7.32–7.19 (m, 4H), 2.52 (s, 3H). ^{13}C NMR ($CDCl_3$, 100 MHz): δ 152.15, 137.15, 131.36, 129.82, 129.63, 126.13, 122.79, 20.91. Anal. Calcd for $C_{14}H_{12}N_2$: C, 80.74; H, 5.81; N, 13.45; found C, 80.74; H, 5.80; N, 13.44.

2-(*m*-Methoxyphenyl)-benzimidazole (3d)[45]

White solid; yield: 90%; mp = 202–204 °C; ^{1}H NMR (DMSO-d_6, 400 MHz): δ 7.72–7.71 (d, J = 6.75 Hz, 2H), 7.58–7.56 (m, 2H), 7.45–7.41 (t, J = 8.25 Hz, 1H), 7.20–7.18 (m, 2H), 7.05–7.03 (m, 1H). ^{13}C NMR (DMSO-d_6, 100 MHz): δ 160.01, 151.49, 131.86, 130.56, 122.62, 119.19, 116.35, 111.84, 55.76. Anal. Calcd for $C_{14}H_{12}N_2O$: C, 74.98; H, 5.39; N, 12.49; found C, 75.01; H, 5.41; N, 12.51.

2-(*p*-Methoxyphenyl)-benzimidazole (3e)[40]

Colourless solid; yield: 87%; mp = 219–221 °C; ^{1}H NMR (DMSO-d_6, 400 MHz): δ 8.30–8.28 (d, J = 8.11 Hz, 1H), 7.93–7.91 (d, J = 8.79 Hz, 1H), 7.69–7.67 (d, J = 8.25 Hz, 1H), 7.42–7.39 (m, 2H), 7.11–7.08 (m, 2H), 6.70–6.68 (d, J = 8.66, 1H). ^{13}C NMR (DMSO-d_6, 100 MHz): δ 162.01, 150.23, 135.57, 130.26, 128.88, 125.23, 123.84, 114.39, 55.37; HRMS (ESI): calcd $[M + H]^+$ 225.1023; found 225.1025; Anal. Calcd for $C_{14}H_{12}N_2O$: C, 74.98; H, 5.39; N, 12.49; found C, 74.95; H, 5.37; N, 12.48.

2-(*m*-Bromophenyl)-benzimidazole (3f)[41]

Colourless solid; yield: 93%; mp = 248–250 °C; ^{1}H NMR (DMSO-d_6, 400 MHz): δ 13.05 (s, 1H), 8.39 (s, 1H), 8.21–8.19 (d, J = 7.75 Hz, 1H), 7.69–7.49 (m, 4H), 7.24–7.22 (m, 2H). ^{13}C NMR (DMSO-d_6, 100 MHz): δ 150.07, 132.87, 131.53, 129.36, 125.83, 122.73. Anal. Calcd for $C_{13}H_9BrN_2$: C, 57.17; H, 3.32; N, 10.26; found C, 57.21; H, 3.34; N, 10.29.

2-(*p*-Bromophenyl)-benzimidazole (3g)[42]

White solid; yield: 94%; mp = 293–295 °C; ^{1}H NMR (DMSO-d$_6$, 400 MHz): δ 8.08–8.06 (d, J = 8.75 Hz, 2H), 7.73–7.72 (d, J = 8.50 Hz, 2H), 7.57–7.55 (m, 2H), 7.18–7.16 (m, 2H). ^{13}C NMR (DMSO-d$_6$, 100 MHz): δ 150.64, 132.45, 129.76, 128.83, 123.75, 122.84. Anal. Calcd for $C_{13}H_9BrN_2$: C, 57.17; H, 3.32; N, 10.26; found C, 57.18; H, 3.33; N, 10.27.

2-(*p*-Chlorophenyl)-benzimidazole (3h)[45]

White solid; yield: 95%; mp = 292–294 °C; ^{1}H NMR (DMSO-d$_6$, 400 MHz): δ 8.19–8.18 (d, J = 8.50 Hz, 2H), 7.65–7.60 (m, 4H), 7.24–7.22 (m, 2H). ^{13}C NMR (DMSO-d$_6$, 100 MHz): 150.59, 135.01, 129.54, 128.61, 122.84. Anal. Calcd for $C_{13}H_9ClN_2$: C, 68.28; H, 3.97; N, 12.25; found C, 68.24; H, 3.94; N, 12.22.

2-(*p*-Fluorophenyl)-benzimidazole (3i)[42]

White solid; yield: 95%; mp = 248–250 °C; ^{1}H NMR (DMSO-d$_6$, 400 MHz): ^{1}H NMR (DMSO-d$_6$, 400 MHz): δ 12.95 (s, 1H), 8.26–8.23 (m, 2H), 7.68–7.54 (m, 2H), 7.43–7.38 (t, J = 8.88 Hz, 2H), 7.22–7.21 (d, J = 3 Hz 2H). ^{13}C NMR (DMSO-d$_6$, 100 MHz): δ 164.75, 162.29, 150.86, 144.23, 135.49, 129.22–129.13 (d, J = 8.72 Hz), 127.28–127.26 (d, J = 2.18 Hz), 122.99, 122.17, 119.30, 116.56, 116.34, 111.77. Anal. Calcd for $C_{13}H_9FN_2$: C, 73.57; H, 4.27; N, 13.20; found C, 73.55; H, 4.26; N, 13.20.

2-(*m*-Nitrophenyl)-benzimidazole (3j)[41]

Yellow solid; yield: 95%; mp = 282–284 °C; ^{1}H NMR (DMSO-d$_6$, 400 MHz): δ 9.02 (s, 1H), 8.63–8.61 (d, J = 7.75 Hz, 1H), 8.35–8.32 (m, 1H), 7.88–7.84 (t, 1H), 7.67–7.65 (m, 2H), 7.28–7.26 (m, 2H). ^{13}C NMR (DMSO-d$_6$, 100 MHz): δ 149.48, 148.82, 132.96, 132.12, 131.17, 124.72, 123.21, 121.32; HRMS (ESI): calcd [M + H]$^+$ 240.0768; found 240.0788; Anal. Calcd for $C_{13}H_9N_3O_2$: C, 65.27; H, 3.79; N, 13.38; found C, 65.29; H, 3.80; N, 13.39.

2-(*p*-Nitrophenyl)-benzimidazole (3k)[43]

Yellow solid; yield: 93%; mp = 301–303 °C; ^{1}H NMR (DMSO-d$_6$, 400 MHz): δ 13.22 (s, 1H), 8.41 (s, 4H), 7.66 (s, 2H), 7.27–7.25 (m, 2H). ^{13}C NMR (DMSO-d$_6$, 100 MHz): 149.44, 148.29, 136.45, 127.88, 124.78, 123.47. Anal. Calcd for $C_{13}H_9N_3O_2$: C, 65.27; H, 3.79; N, 13.38; found C, 65.28; H, 3.81; N, 13.37.

2-(*N*,*N*-Dimethylaminophenyl)-benzimidazole (3l)[44]

Yellow solid; yield: 92%; mp = 229–231 °C; ^{1}H NMR (DMSO-d$_6$, 400 MHz): δ 8.04–8.02 (d, J = 8.50 Hz, 2H), 7.54–7.52 (m, 2H), 7.15–7.13 (m, 2H), 6.84–6.82 (d, J = 8.75 Hz, 2H), 2.98 (s, 6H). ^{13}C NMR (DMSO-d$_6$, 100 MHz): δ 152.77, 151.69, 128.03, 121.83, 117.81, 112.29; HRMS (ESI): calcd [M + H]$^+$ 238.1339; found 238.1335; Anal. Calcd for $C_{15}H_{15}N_3$: C, 75.92; H, 6.37; N, 17.71; found C, 75.89; H, 6.36; N, 17.70.

2-(*m*-Chlorophenyl)-benzimidazole (3m)[45]

White solid; yield: 92%; mp = 227–229 °C; ^{1}H NMR (DMSO-d$_6$, 400 MHz): δ 8.24 (s, 1H), 8.17–8.15 (m, 1H), 7.64–7.56 (m, 4H), 7.26–7.23 (m, 2H). ^{13}C NMR (DMSO-d$_6$, 100 MHz): δ 150.11, 134.32, 131.54, 130.33, 126.48, 125.49, 115.67. Anal. Calcd for $C_{13}H_9ClN_2$: C, 68.28; H, 3.97; N, 12.25; found C, 68.31; H, 3.98; N, 12.26.

2-(Furan-2-yl)-benzimidazole (3n)[40]

Pale yellow solid; yield: 91%; mp = 290–292 °C; ^{1}H NMR (DMSO-d$_6$, 400 MHz): δ 13.02 (s, 1H), 7.94 (d, J = 1 Hz, 1H), 7.58–7.56 (m, 1H), 7.22–7.19 (m, 4H), 6.74–6.72 (m, 1H). ^{13}C NMR (DMSO-d$_6$, 100 MHz): δ 146.02, 145.07, 144.09, 122.68, 112.77, 110.95; HRMS (ESI): calcd [M + H]$^+$ 185.0710; found 185.0680; Anal. Calcd for $C_{11}H_8N_2O$: C, 71.73; H, 4.38; N, 15.21; found C, 71.69; H, 4.37; N, 15.19.

Author contributions

S. K., G. R., S. H., and R. C. designed the schemes. S. K. performed the experiments. S. K., and G. R. evaluated the data and prepared the figures and tables. G. R., S. K., S. H., and R. C. revised and reviewed the manuscript.

Conflicts of interest

The authors declare no competing financial interest.

Acknowledgements

S. K. acknowledges CSIR for the award of Junior Research Fellowship (File No: 09/045(1671)/2019-EMR-I) and is also thankful to the University of Delhi, India-110007.

References

1 F. Gualtieri, G. Brody, A. H. Fieldsteel and W. A. Skinner, *J. Med. Chem.*, 1972, **15**, 420–422.
2 W. A. Denny, G. W. Rewcastle and B. C. Bauley, *J. Med. Chem.*, 1990, **33**, 814–819.
3 G. Kaur, M. Kaur and O. Silakari, *Mini-Rev. Med. Chem.*, 2014, **14**, 747–767.
4 J. L. Wang, J. Zhang, Z. M. Zhou, Z. H. Li, W.-Z. Xue, D. Xu, L. P. Hao, X. F. Han, F. Fei, T. Liu and A. H. Liang, *Eur. J. Med. Chem.*, 2012, **49**, 183.
5 B. Fang, C. H. Zhou and X. C. Rao, *Eur. J. Med. Chem.*, 2010, **45**, 4388–4398.
6 E. Cereda, M. Turconi, A. Ezhaya, E. Bellora, A. Brambilla, F. Pagani and A. Donetti, *Eur. J. Med. Chem.*, 1987, **22**, 527.
7 A. Figge, H. J. Altenbach, D. J. Brauer and P. Tielmann, *Tetrahedron: Asymmetry*, 2002, **13**, 137–144.
8 (*a*) N. Manjunatha, M. Imadadulla, K. S. Lokesh and K. V. Reddy, *Dyes Pigm.*, 2018, **153**, 213–224; (*b*) Y. C. Wang, L. Z. Liu, Y. M. Pan and H. S. Wang, *Molecules*, 2011, **16**, 100–106; (*c*) S. Suresh, K. Jayamoorthy and S. Karthikeyan, *J. Lumin.*, 2018, **198**, 28–33; (*d*) I. Milošev, N. Kovačević and A. Kokalj, *Acta Chim. Slov.*, 2016, **63**, 544–559.

9 (*a*) E. C. Wagner and W. H. Millett, *Org. Synth.*, 2003, **19**, 12–12; (*b*) J. B. Wright, *Chem. Rev.*, 1951, **48**, 397–541; (*c*) P. N. Preston, *Chem. Rev.*, 1974, **74**, 279–314; (*d*) K. J. Lee and K. D. Janda, *Can. J. Chem.*, 2001, **79**, 1556–1561; (*e*) M. Curini, F. Epifano, F. Montanari, O. Rosati and S. Taccone, *Synlett*, 2004, 1832–1834; (*f*) K. Bahrami, M. M. Khodaei and I. Kavianinia, *Synthesis*, 2007, 547–550.

10 F. Feng, J. Ye, Z. Cheng, X. Xu, Q. Zhang, L. Ma, C. Lu and X. Li, *RSC Adv.*, 2016, **6**, 72750–72755.

11 P. V. G. Reddy, B. R. P. Reddy, M. V. K. Reddy, K. R. Reddy, N. P. Shetti, T. A. Saleh and T. M. Aminabhavi, *J. Environ. Manage.*, 2020, 111603.

12 (*a*) J. M. Campelo, D. Luna, R. Luque, J. M. Marinas and A. A. Romero, *ChemSusChem*, 2009, **2**, 18–45; (*b*) M. Rawat and D. S. Rawat, *Tetrahedron Lett.*, 2019, **60**, 1153–1157.

13 P. Munnik, P. E. de Jongh and K. P. de Jong, *Chem. Rev.*, 2015, **115**, 6687–6718.

14 C. Lancelot, V. V. Ordomsky, O. Stéphan, M. Sadeqzadeh, H. Karaca, M. Lacroix, D. Curulla-Ferré, F. Luck, P. Fongarland, A. Griboval-Constant and A. Y. Khodakov, *ACS Catal.*, 2014, **12**, 4510–4515.

15 Z. Chen, J. Mao and R. Zhou, *Appl. Surf. Sci.*, 2019, **465**, 15–22.

16 R. Rezaei, G. Moradi and S. Sharifnia, *Energy Fuels*, 2019, **33**, 6689–6706.

17 D. W. Hatchett and M. Josowicz, *Chem. Rev.*, 2008, **108**, 746–769.

18 E. N. Prabhakaran and J. Iqbal, *J. Org. Chem.*, 1999, **64**, 3339–3341.

19 G. Evano, N. Blanchard and M. Toumi, *Chem. Rev.*, 2008, **108**, 3054–3131.

20 H. Huang, W. Huang, Y. Xu, X. Ye, M. Wu, Q. Shao, G. Ou, Z. Peng, J. Shi, J. Chen, Q. Feng, Y. Zan, H. Huang and P. Hu, *Catal. Today*, 2015, **258**, 627–633.

21 A. Ahmed, P. Elvati and A. Violi, *RSC Adv.*, 2015, **5**, 35033–35041.

22 J. Mondal, A. Biswas, S. Chiba and Y. Zhao, *Sci. Rep.*, 2015, **5**, 8294.

23 M. B. Gawande, A. Goswami, F. X. Felpin, T. Asefa, X. Huang, R. Silva, X. Zou, R. Zboril and R. S. Varma, *Chem. Rev.*, 2016, **116**, 3722–3811.

24 (*a*) M. L. Kantam, C. V. Reddy, P. Srinivas and S. Bhargava, *Amination and Formation of sp2 CN Bonds*, 2013, pp. 119–171; (*b*) *Copper-mediated cross-coupling reactions*, ed. G. Evano and N. Blanchard, Wiley, Hoboken, NJ, 2014.

25 (*a*) R. Arundhathi, D. Damodara, K. V. Mohan, M. L. Kantam and P. R. Likhar, *Adv. Synth. Catal.*, 2013, **355**, 751–756; (*b*) A. R. Hajipour, F. Dordahan, F. Rafiee and M. Mahdavi, *Appl. Organomet. Chem.*, 2014, **28**, 809–813; (*c*) P. L. Reddy, R. Arundhathi and D. S. Rawat, *RSC Adv.*, 2015, 92121–92127; (*d*) S. Frindy, A. el Kadib, M. Lahcini, A. Primo and H. García, *ChemCatChem*, 2015, **7**, 3307–3315; (*e*) P. Puthiaraj and W. S. Ahn, *Catal. Sci. Technol.*, 2016, **6**, 1701–1709; (*f*) V. Gutierrez, E. Mascaró, F. Alonso, Y. Moglie and G. Radivoy, *RSC Adv.*, 2015, **5**, 65739–65744.

26 (*a*) F. Alonso, T. Melkonian, Y. Moglie and M. Yus, *Eur. J. Org. Chem.*, 2011, 2524–2530; (*b*) F. Alonso, A. Arroyo, I. Martin-Garcia and Y. Moglie, *Adv. Synth. Catal.*, 2015, **357**, 3549–3561.

27 (*a*) T. Jin, M. Yan and Y. Yamamoto, *ChemCatChem*, 2012, **4**, 1217–1229; (*b*) F. Alonso, Y. Moglie and G. Radivoy, *Acc. Chem. Res.*, 2015, **48**, 2516–2528; (*c*) M. J. Albaladejo, F. Alonso and M. J. González-Soria, *ACS Catal.*, 2015, **5**, 3446–3456.

28 G. Rathee, S. Kohli, N. Singh, A. Awasthi and R. Chandra, *ACS Omega*, 2020, **5**, 15673–15680.

29 G. Rathee, S. Kohli, S. Panchal, N. Singh, A. Awasthi, S. Singh, A. Singh, S. Hooda and R. Chandra, *ACS Omega*, 2020, **5**, 23967–23974.

30 (*a*) X. Wang, Y. Shen, A. Xie, L. Qiu, S. Li and Y. Wang, *J. Mater. Chem.*, 2011, **21**, 9641–9646; (*b*) X. Wang, J. Zhang, K. Zhang, W. Zou and S. Chen, *RSC Adv.*, 2016, **50**, 44851–44858.

31 P. D. Kirsch and J. G. Ekerdt, *J. Appl. Phys.*, 2001, **90**, 4256–4264.

32 (*a*) S. A. Mirfarjood, M. Mamaghani and M. Sheykhan, *J. Nanostruct. Chem.*, 2017, **4**, 359–366; (*b*) J. Azizian, P. Torabi and J. Noei, *Tetrahedron Lett.*, 2016, **2**, 185–188; (*c*) J. Yu, J. Xu and M. Lu, *Appl. Organomet. Chem.*, 2013, **10**, 606–610.

33 S. Azeez, P. Sureshbabu, P. Chaudhary, S. Sabiah and J. Kandasamy, *Tetrahedron Lett.*, 2020, **61**, 151735.

34 C. Chaudhari, S. H. Siddiki and K. I. Shimizu, *Tetrahedron Lett.*, 2015, **56**, 4885–4888.

35 P. L. Reddy, R. Arundhathi, M. Tripathi and D. S. Rawat, *RSC Adv.*, 2016, **6**, 53596–53601.

36 D. Yang, X. Zhu, W. Wei, N. Sun, L. Yuan, M. Jiang, J. You and H. Wang, *RSC Adv.*, 2014, **4**, 17832–17839.

37 N. V. Shitole, K. S. Niralwad, B. B. Shingate and M. S. Shingare, *Arabian J. Chem.*, 2016, **9**, S858–S860.

38 M. Jafarpour, A. Rezaeifard, M. Ghahramaninezhad and T. Tabibi, *New J. Chem.*, 2013, **37**, 2087–2095.

39 S. M. Inamdar, V. K. More and S. K. Mandal, *Tetrahedron Lett.*, 2013, **54**, 579–583.

40 A. J. Blacker, M. M. Farah, M. I. Hall, S. P. Marsden, O. Saidi and J. M. Williams, *Org. Lett.*, 2009, **11**, 2039–2042.

41 M. Shamsi-Sani, F. Shirini, M. Abedini and M. Seddighi, *Chem. Intermed.*, 2016, **42**, 1091–1099.

42 M. Karthik and P. Suresh, *New J. Chem.*, 2018, **42**, 17931–17938.

43 K. Bahrami and M. Bakhtiarian, *ChemistrySelect*, 2018, **3**, 10875–10880.

44 S. V. Ryabukhin, A. S. Plaskon, D. M. Volochnyuk and A. A. Tolmachev, *Synthesis*, 2006, 3715–3726.

45 Z. Geng, H. Y. Zhang, G. Yin, Y. Zhang and J. Zhao, *J. Chem. Res.*, 2020, **44**, 557–565.